energies

MDPI

Article

Validation of a Holistic System for Operational Analysis and Provision of Ancillary Services in Active Distribution Networks

Theofilos A. Papadopoulos [1,*], Kalliopi D. Pippi [1], Georgios A. Barzegkar-Ntovom [1], Eleftherios O. Kontis [2], Angelos I. Nousdilis [2], Christos L. Athanasiadis [1] and Georgios C. Kryonidis [2]

[1] Department of Electrical & Computer Engineering, Democritus University of Thrace, 67100 Xanthi, Greece; kpippi@ee.duth.gr (K.D.P.); gbarzegk@ee.duth.gr (G.A.B.-N.); cathanas@ee.duth.gr (C.L.A.)
[2] School of Electrical & Computer Engineering, Aristotle University of Thessaloniki, 54124 Thessaloniki, Greece; ekontis@auth.gr (E.O.K.); angelos@ece.auth.gr (A.I.N.); kryonidi@ece.auth.gr (G.C.K.)
* Correspondence: thpapad@ee.duth.gr

Abstract: The advent of distributed renewable energy sources (DRESs) has led to the progressive transformation of traditional distribution networks to active components of the power system. This transformation, however, may jeopardize the reliable grid operation due to the advent of new technical problems, such as network overloading, over-/under-voltage events, abnormal frequency deviation and dynamic instability. In this challenging scenery, the installation of a modern measuring infrastructure has created new sources of data and information that facilitate the provision of ancillary services (ASs) via measurement-based analysis. The ACTIVATE (ancillary services in active distribution networks based on monitoring and control techniques) project aims to design innovative AS solutions for power system operators. These solutions aim to tackle the technical issues emerged by the ever-increasing DRES penetration and their volatile nature. In this context, in ACTIVATE, a holistic system is proposed comprising centralized and decentralized control features to enhance the overall network performance. Additionally, a network monitoring system is designed to support a number of online and offline dynamic analysis applications by exploiting measurements obtained at the transmission, primary and secondary distribution network. This paper presents a validation of the overall system, which is performed by using simulation and power-hardware-in-the-loop results in combined transmission and distribution network models.

Keywords: ancillary services; congestion management; distributed generation; equivalent models; measurement-based analysis techniques; mode estimation; power smoothing; voltage regulation; voltage unbalance

Citation: Papadopoulos, T.A.; Pippi, K.D.; Barzegkar-Ntovom, G.A.; Kontis, E.O.; Nousdilis, A.I.; Athanasiadis, C.L.; Kryonidis, G.C. Validation of a Holistic System for Operational Analysis and Provision of Ancillary Services in Active Distribution Networks. *Energies* **2023**, *16*, 2787. https://doi.org/10.3390/en16062787

Academic Editor: Alon Kuperman

Received: 6 February 2023
Revised: 7 March 2023
Accepted: 10 March 2023
Published: 17 March 2023

1. Introduction

The advent of renewable energy sources (RESs) either in the form of large-scale plants or distributed renewable energy sources (DRESs) has posed unprecedented technical challenges to system operators, i.e., transmission system operators (TSOs) and distribution system operators (DSOs), jeopardizing the reliable operation of both the transmission (TN) and distribution networks (DNs). In this context, ancillary services (ASs), i.e., the set of functions that help grid operators maintain a reliable electricity system, are expected to be delivered from both large-scale RESs connected at the TN and small-scale DRESs installed at the DN level [1–6].

In the near future, two types of ASs are foreseen: (i) DN-oriented AS and (ii) TN-oriented AS [7]. In terms of DN-oriented ASs, DSOs coordinate the operation of DRESs with the aid of local storage systems, e.g., battery energy storage (BES) to tackle local long-duration problems [8] and to deal with the ever-increasing voltage fluctuation problem caused by the intermittent nature of DRESs [9]. In this aspect, DSO-oriented ASs involve mainly voltage regulation (VR), voltage unbalance mitigation (VUM), congestion management (CM), and power smoothing (PS). In particular, VR refers to control methods tackling

potential under- and overvoltages, and VUM to voltage asymmetry problems. CM algorithms alleviate overloads on the main network components, and PS includes techniques related to smoothing the output power of DRESs with variable primary sources, e.g., wind turbines and photovoltaics (PVs). TSO-oriented ASs are provided at the TN level by coordinating the operation of large scale RES and DRES to solve issues having a wider impact on the power system, e.g., reactive power support, PS and dynamic stability improvement [7].

In addition, to facilitate the development of ASs and exploit the flexibility offered by large-scale RES and DRES, online monitoring systems are used by system operators to monitor, analyze, and control, in close to real time, their grids [7,10]. Originally, online wide-area monitoring systems [11] pertain to the TN level, where measurements from several network buses, recorded via phasor measurement units (PMUs), are gathered at a phasor data concentrator (PDC). In the PDC, measurement-based identification techniques are applied to develop reduced order equivalents to derive modal components, to estimate the dynamic characteristics of the grid and finally to assess the stability margins [11,12]. Nowadays, with the emergence of different monitoring architectures at the DN level, the application of measurement-based techniques has been even further extended [10].

In this context, the ACTIVATE (ancillary services in active distribution networks based on monitoring and control techniques) project [13] targets the development of novel AS solutions within a holistic framework. The core of the system is a set of hybrid control strategies, combining features of centralized and decentralized architectures to improve the network operation in terms of VR, VUM, CM and PS. For this purpose, the functionalities that the network assets offer are exploited, including BES and the new operational features of inverter based resources (IBR), i.e., DRES and BES. In addition, in order to monitor and analyze the power system dynamics, a network monitoring system is incorporated to support a number of online (e.g., mode estimation) and offline (e.g., DN equivalencing) dynamic analysis applications based on autoregressive–moving average with exogenous inputs (ARMAX) modeling. This paper extends previous studies [10,14,15] and presents validation results of the overall proposed system. Concurrent quasi-static and dynamic analysis simulation results are used in a combined transmission and distribution (T&D) network model to evaluate the performance of the hybrid control strategies and the online and offline applications, respectively. The network monitoring system performance is also tested in a power hardware-in-the-loop (PHIL) simulation environment. The explicit contributions of the analysis are summarized in the following aspects:

1. The VUM, VR, CM schemes of [14] and the PS techniques of [15] are integrated into a holistic hybrid control strategy to constitute a unified ASs framework.
2. The ASs framework is applied to solve realistic problems in large-scale studies, including both primary and secondary DNs.
3. The efficiency of the proposed hybrid control strategies is validated for different operating conditions via quasi-static simulations.
4. Dynamic equivalent models (DEM) [10] are implemented and incorporated into simulation models.
5. The impact of IBRs and load modeling on the dynamic performance of DNs is investigated.
6. The mode estimation algorithm of [10] for small-signal analysis is evaluated by using the PHIL results.

Bearing the above remarks in mind, the paper is organized as follows: Section 2 first provides an overview of the holistic hybrid strategy and its constituent parts, i.e., the VUM, VR, CM and PS control schemes. In Section 3, the most important ACTIVATE network monitoring system applications are described, i.e., mode estimation and dynamic equivalent modeling. Section 4 provides details on the simulation model. In particular, in Section 4.1 the topology of the T&D network is described; the adopted models of DRES, BES and loads for the quasi-static and the dynamic analysis are presented in Section 4.2 and Section 4.3, respectively. By using the quasi-static models, the efficacy of the overall hybrid control strategy is verified with simulation results in Section 5. In Section 6, the accuracy of

the developed DEM is evaluated, and the effect of IBRs and load modeling on the system dynamic performance is also investigated by means of time-domain simulations. Small-signal analysis is studied in the PHIL setup of Section 7. Finally, Section 8 summarizes the most important conclusions of the paper.

2. Proposed Ancillary Services

2.1. Hybrid Control Strategy

The conceptual representation of the ACTIVATE hybrid strategy for AS provision is depicted in Figure 1. It comprises four control blocks each supported by a dedicated control algorithm for VR, CM, VUM [14] and PS [15], respectively. As a common characteristic, these control algorithms are data driven, i.e., their control actions are determined based only on information received by local and/or remote measurements within the grid. This way, the performance of the proposed solution for AS provision is not affected by potential modeling uncertainties, e.g., use of forecast data. The provided ASs are coordinated by means of a two-layer hierarchical architecture. The following provide more detail:

- Central controller (CC) layer: The CC is employed to coordinate the operation of DRES/BES units via their local controllers (LCs) by sending control signals in case of voltage violation and/or current overload events. The CC coordination concept is depicted in Figures 2 and 3 for the primary and the secondary DN, respectively.
- Local controller (LC) layer: LCs are integrated into the DRES/BES converters and exchange information with the CC on a regular basis. The operation of the LC is sub-divided into the DRES and the BES LC layer (Figure 3). Note that, a dedicated converter is considered for each of the DRES and the BES units (see Figure 3). The DRES LC is responsible for adjusting the DRES converter output power based only on the measurements acquired at point of interconnection (POI) to address potential voltage violations and asymmetries as well as current overloads. In addition, to smooth out possible DRES power fluctuations, a PS algorithm is applied and the BES is used to cover the power mismatch between the maximum power point (MPP) generated from the DRES and the injected smoothed power to the grid. For this purpose, and also as a supplementary solution for CM, VR and VUM the BES LC at the BES converter is used.

The hierarchical architecture layers and the control algorithms are discussed in detail in the following subsections.

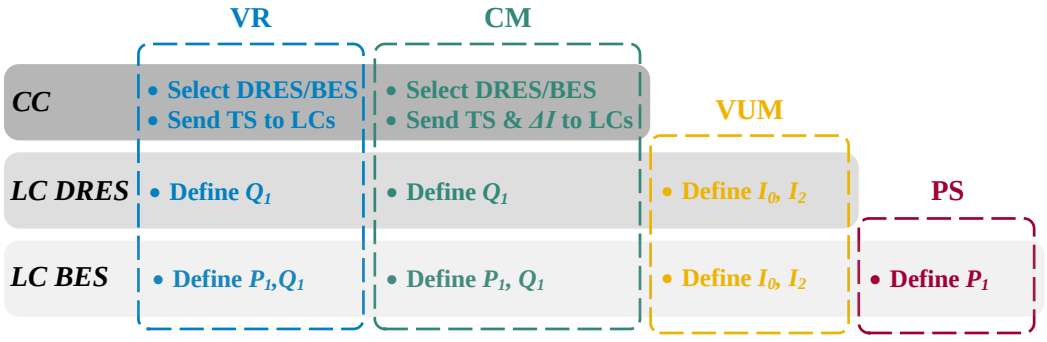

Figure 1. Conceptual representation of the hybrid strategy.

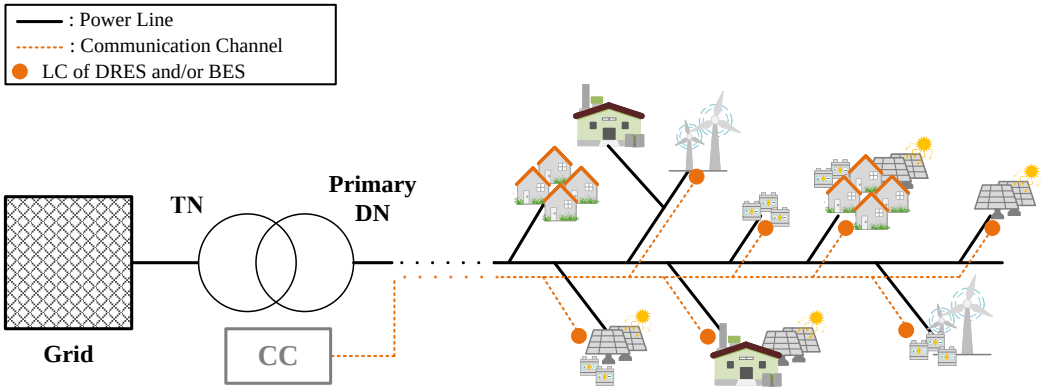

Figure 2. System architecture in primary DNs.

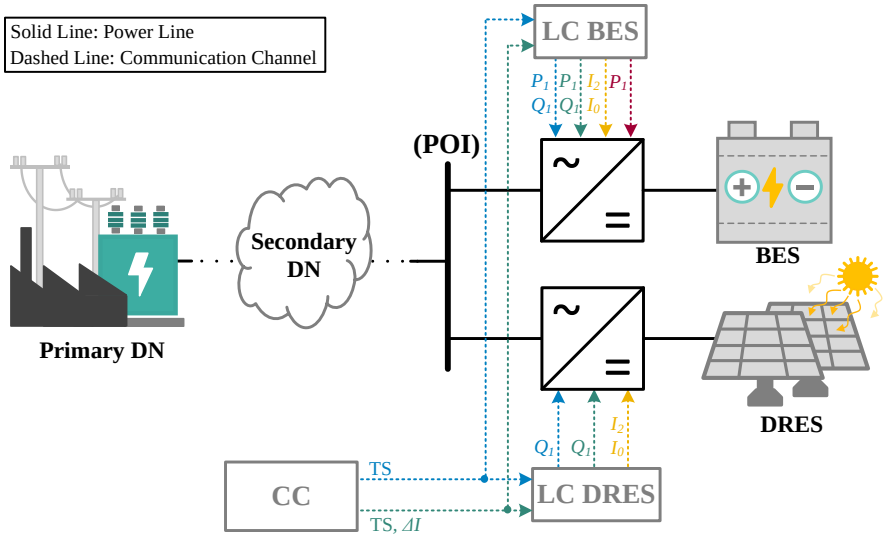

Figure 3. System architecture in secondary DNs.

2.2. Power Smoothing Technique

To compensate the DRES power fluctuations, the generic PS scheme [16,17] of Figure 4 is adopted. It consists of a ramp-rate limitation (RRL) algorithm and a state-of-charge (*SoC*) recovery mechanism. The target of the RRL control is to maintain the ramp rate, RR^t, of the generated at MPP PV output power, P^t_{mpp}, within specific minimum, $RR_{\min}$, and maximum, $RR_{\max}$, limits. The former is introduced to limit ramp-downs, i.e., negative ramp rates caused by the reduction in the DRES output power, and the latter to limit ramp-ups, i.e., positive ramp rates due to the increase of the DRES output power. The RR^t at time instant t in W/s is defined as

$$RR^t = \frac{P^t_{in} - P^{t-\Delta t}_s}{\Delta t} \tag{1}$$

where P^t_{in} is the power introduced to the RRL control (see Figure 4) and $P^{t-\Delta t}_s$ is the smoothed power at $t - \Delta t$. This way, the smoothed power P^t_s at t results from (2):

$$P^t_s = \begin{cases} P^{t-\Delta t}_s + \Delta t \cdot RR_{\min}, & RR^t \leq RR_{\min} \\ P^{t-\Delta t}_s + \Delta t \cdot RR^t, & RR_{\min} < RR^t < RR_{\max} \\ P^{t-\Delta t}_s + \Delta t \cdot RR_{\max}, & RR^t \geq RR_{\max}. \end{cases} \tag{2}$$

The BES unit charges or discharges to cover the power mismatch difference $P^t_{bat} = P^t_{mpp} - P^t_s$. Eventually, the stored or drained BES energy within Δt depends on P_{bat} and the battery charging or discharging efficiency, η_{ch} or η_{dch}, respectively. However, the uneven distribution between ramp-ups and ramp-downs lead to different amounts of

energy that need to be stored or drained from the BES unit [18]. As a result, the permissible *SoC* limits can be reached, jeopardizing the PS process. To overcome this issue, a *SoC* recovery mechanism is added to the RRL control, as shown in Figure 4. The scope of this mechanism is to ensure that BES unit operates away from the *SoC* limits, thus being available to smooth out the PV output variations. This is attained by introducing a proportional feedback control. Specifically, the error between the actual stored BES energy at time instant t, E_{bat}^{t}, and a reference value, E_{BES}^{ref}, is multiplied by the proportional term, k, and is forwarded back to the control input prior to the ramp-rate limiter. As the value of k increases, a faster *SoC* recovery is achieved; typical values for k are within the range of 0.5 h^{-1} to 3 h^{-1}.

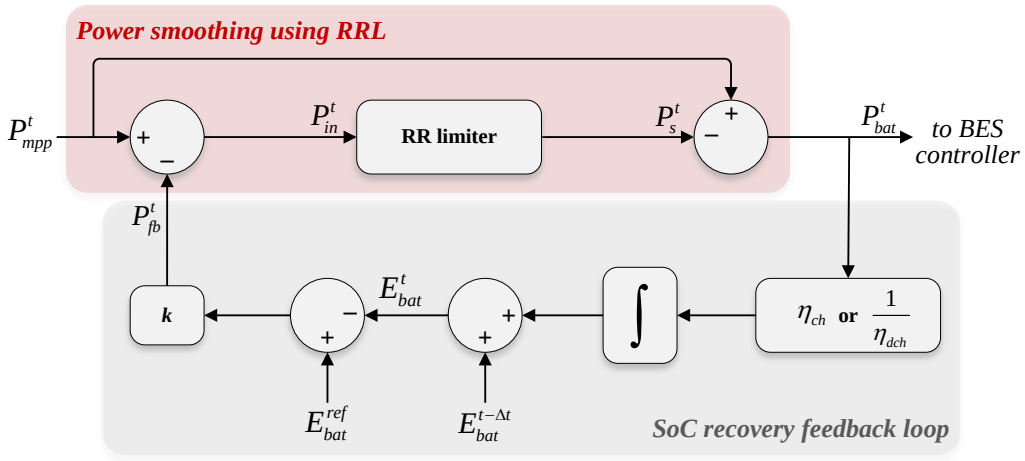

Figure 4. Enhanced RRL-based PS technique with *SoC* recovery.

2.3. VUM Scheme

Voltage unbalances in secondary DNs are mitigated by using the reactive power capability of the DRES and/or BES converter. Reactive power is exploited to reduce the BES utilization and ensure that VUM is available in case the active power of DRES/BES is not available. In this sense, VUM can be always activated ensuring the effective reduction of network unbalances. Note that the virtual admittance concept is adopted for controlling the DRES/BES converter [19]. According to this, the output currents of the DRES/BES converter are determined by multiplying the POI voltage with a virtual admittance. In this paper, the virtual admittance matrix **Y** is introduced as follows:

$$\begin{bmatrix} \bar{I}_0 \\ \bar{I}_1 \\ \bar{I}_2 \end{bmatrix} = \underbrace{\begin{bmatrix} \bar{Y}_0 & 0 & 0 \\ 0 & \bar{Y}_1 & 0 \\ 0 & 0 & \bar{Y}_2 \end{bmatrix}}_{\mathbf{Y}} \begin{bmatrix} \bar{V}_0 \\ \bar{V}_1 \\ \bar{V}_2 \end{bmatrix}. \tag{3}$$

where $\bar{I}_y$ and $\bar{V}_y$ denote the symmetrical component output currents and POI voltages of the DRES/BES converter (see Figure 3), respectively. By setting the non-diagonal elements of **Y** equal to zero, it is evident that the symmetrical components are decoupled, rendering feasible the individual control of the symmetrical component currents [14]. It must be also indicated that in order to compensate the voltage unbalance, only the reactive capability of the converter is exploited by means of $\bar{Y}_0 = jB_0$ and $\bar{Y}_2 = jB_2$, leaving intact the output active power of both DRES and BES. Finally, $\bar{Y}_1$ is determined by the outputs of the VR strategy analyzed in Section 2.4.

2.4. VR Strategy

An event-triggered VR strategy is proposed to solve overvoltage and undervoltage issues. The proposed VR is based on the coordinated operation of the CC and the DRES/BES

LCs as depicted in the flowcharts of Figure 5. In particular, the DRES/BES LCs communicate on a regular basis with the CC and transmit their measured at POI positive-sequence voltage, V_1 and an auxiliary binary variable b_{aux} (See Figure 5a). From the obtained data, the CC identifies the nodes exceeding $V_{\text{lim}}^{\max}$ (assuming network overvoltage) and activates the VR algorithm at the LC node, presenting the maximum overvoltage by sending appropriate activation signals (See Figure 5b).

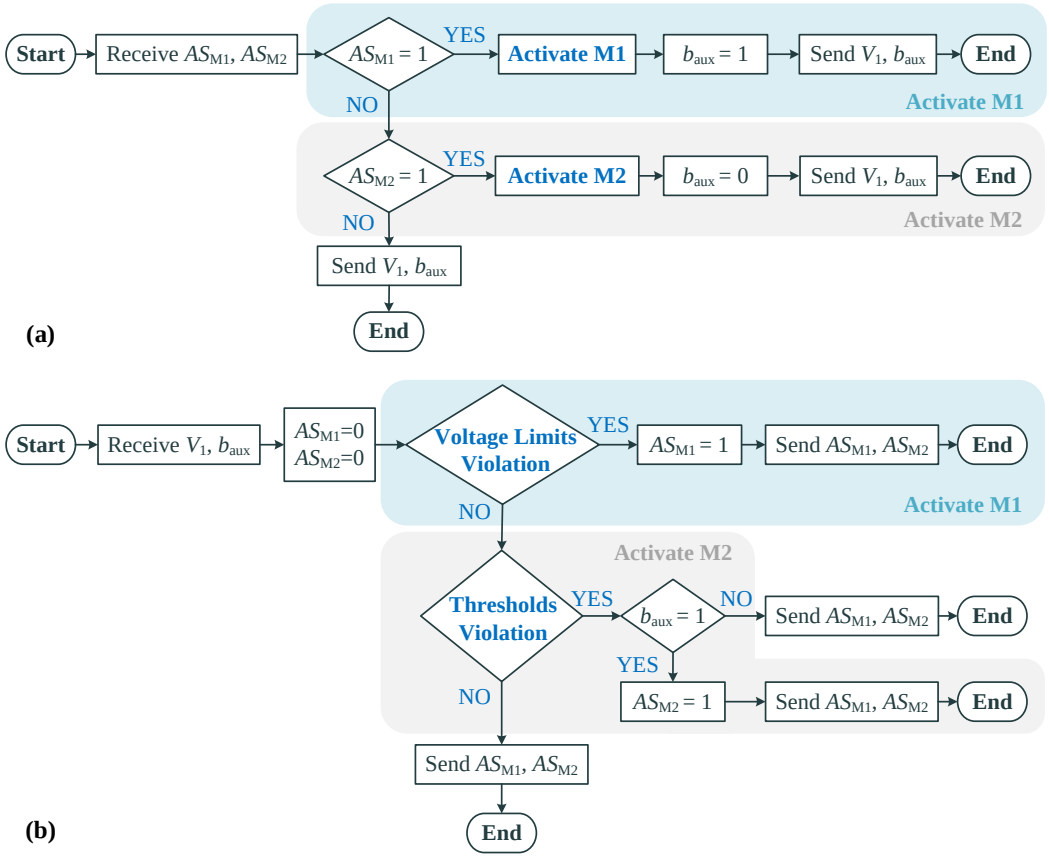

Figure 5. Operation schemes of (**a**) the LCs and (**b**) the CC.

The proposed VR algorithm consists of two operational modes, i.e., M1 and M2. M1 is used to regulate V_1 at POI within predefined limits by prioritizing the use of Q_1 instead of P_1; P_1 and Q_1 pertain to positive-sequence power. In case a voltage violation occurs, the activation signal, AS_{M1}, is transmitted from the CC to the LC. The latter sends back a $b_{\text{aux}} = 1$ to denote that VR is enabled to the corresponding node. In case $AS_{\text{M1}} = 1$, the available amount of the DRES/BES converter, Q_1, is initially used as the only means for VR. The corresponding reference positive-sequence reactive power, Q_1^{ref}, that should be absorbed/injected is determined by means of (4)

$$Q_1^{\text{ref}} = (V_1 - V_{\text{ref}}) \left(k_{\text{p}}^{\text{VR}} + \frac{k_{\text{i}}^{\text{VR}}}{s} \right) \tag{4}$$

where k_{p}^{VR} and k_{i}^{VR} are the proportional and the integral gains of the converter PI controller, respectively; V_{ref} is the reference voltage level and is equal to $V_{\text{lim}}^{\max} - 0.5db$, in case of an overvoltage incident, or $V_{\text{lim}}^{\min} + 0.5db$ for undervoltage events. Note that the deadband, db, is considered between the operation of M1 and M2, in order to avoid possible oscillations and recurrent switching. The process is repeated till either the voltage is regulated or the maximum available reactive power, $Q_{\max}$, is reached, where $Q_{\max}$ is

$$Q_{\max} = \sqrt{S_1^2 - P_1^2}. \tag{5}$$

Here, S_1 is the nominal apparent power of the converter, and P_1 is the active power absorbed/injected by the converter during the control.

If Q_1^{ref} reaches $Q_{\max}$ or the voltage violation event has not been totally mitigated, the VR process proceeds with the P_1 utilization of BES. The required P_1^{ref}, that should be absorbed/injected is estimated by employing an additional PI controller and the Q_1^{ref} is readjusted to a new value according to (5). The process is repeated till either the voltage is regulated, or the maximum available active power, $P_{\max}$, estimated by (6), is reached:

$$P_{\max} = \frac{S_1}{pf} \tag{6}$$

where, pf refers to the nominal power factor of the BES converter.

Once M1 completes, the VR control scheme remains idle. Nevertheless, possible changes in the network operating conditions may result in (i) a decrease in V_1 below the threshold $V_{\text{lim}}^{\max} - db$ (in case where overvoltage incidents were previously observed), or (ii) an increase of V_1 higher than $V_{\text{lim}}^{\min} + db$ (in case where undervoltages were previously detected), and consequently lead to unnecessary power absorption/injection by the converter. For this reason, if $b_{\text{aux}} = 1$, the CC sends another activation signal, i.e., AS_{M2}, to the LC to enable M2. The purpose of M2 is to avoid the unnecessary use of BES by adjusting the P_1 control, until voltage V_1 is regulated or P_1 becomes zero. In the latter case, Q_1 is also reduced to zero ($b_{\text{aux}} = 0$), unless the voltage is regulated.

The VR strategy incorporates also a day-ahead planning algorithm to ensure the successful participation of the DRES/BES systems to the VR process of the next day. Specifically, in the CC, the day-ahead generation and consumption profiles are forecasted, and quasi-static simulations are performed employing the proposed VR method. From the obtained results, the required storage range, SR, i.e., the amount of energy that will be stored during the VR process by each BES in the next day, is predicted [14,15]. A safety factor, sf, is also taken into account in the final estimate. Subsequently, a discharging process with constant power is applied to each BES with non-zero SR during no-generation periods to reach the required storing capability. Note that a similar rationale also applies to undervoltage events.

2.5. CM Strategy

To alleviate overloads in the DN lines, a CM strategy is also considered. In particular, the CC constantly monitors the currents flowing through the network transformer (either HV/MV or MV/LV for the primary and secondary DNs, respectively) and also the lines close to or directly connected to the corresponding transformer downstream busbar. These are considered the most vulnerable to current overloading due to the radial configuration of the majority of distribution grids [20].

In particular, the CC calculates the current deviation (ΔI) from the line ampacity ($\mathbf{I}_{\max}$). If $\Delta I > \mathbf{I}_{\max}$, i.e., the current has crossed the emergency limit, a current overloading is detected, and the following step-by-step procedure is followed:

- **Step 1**: The CC selects the DRES/BES of the node presenting the lowest impact on the network voltages to participate in the CM scheme. This is determined by means of the network sensitivity matrix:

$$\begin{bmatrix} \Delta\boldsymbol{\theta_1} \\ \Delta|\bar{\mathbf{V}}_\mathbf{1}| \end{bmatrix} = \mathbf{J_1^{-1}} \begin{bmatrix} \Delta\mathbf{P_1} \\ \Delta\mathbf{Q_1} \end{bmatrix} = \begin{bmatrix} \mathbf{k} & \mathbf{l} \\ \mathbf{m} & \mathbf{n} \end{bmatrix} \begin{bmatrix} \Delta\mathbf{P_1} \\ \Delta\mathbf{Q_1} \end{bmatrix} \tag{7}$$

  where $\mathbf{J_1^{-1}}$ is the inverse Jacobian matrix in the positive-sequence quantifying the voltage magnitude $\Delta|\bar{\mathbf{V}}_\mathbf{1}|$ and angle ($\Delta\boldsymbol{\theta_1}$) variations with respect to active ($\Delta\mathbf{P_1}$) and

reactive power ($\Delta\mathbf{Q_1}$) fluctuations. **m** and **n** are the sub-matrices of (7) containing the partial derivatives $\partial|\bar{\mathbf{V}}_\mathbf{1}|/\partial\mathbf{P_1}$ and $\partial|\bar{\mathbf{V}}_\mathbf{1}|/\partial\mathbf{Q_1}$, respectively. Using these sub-matrices, the CC can identify the available DRES/BES of the node with the lowest impact of the network voltages. This way, the interaction between the CM and the VR is kept as minimal as possible. Concerning secondary DNs, sub-matrix **m** is considered in the DRES/BES selection process since the network voltages are more sensitive to active power variations due to the high R/X ratio of the lines. On the contrary, in primary DNs, sub-matrix **n** is used in the selection process due to the higher sensitivity of network voltages to reactive power variations. It is worth mentioning that in case either the Jacobian is singular or its condition number exceeds a certain limit, the sensitivity matrix can be estimated using the inversion-free analytical calculations of [21].

- **Step 2**: The CC communicates with the identified LC to adjust its available DRES/BES converter active and reactive power to reduce the currents flowing through the lines.
- **Step 3**: The LC, via a dedicated PI controller, increases the DRES/BES output current as requested by the CC, i.e., ΔI. Additionally in this case, the use of the reactive power is prioritized against active power. Therefore, the BES active power is used only if the BES maximum reactive power has first been reached.
- **Step 4**: If the maximum active power has been reached, the process shifts to the succeeding DRES/BES (according to (7)), having the lowest impact on the network voltages.
- **Step 5**: The procedure repeats till the line overloads have finally been eliminated.

3. Developed Network Monitoring System

The core of the monitoring system is to collect, process, store and analyze measured data from multiple locations of the TN and the DNs. This enables different online and offline applications. A detailed description of the architecture of the network monitoring system is described [10]. Herein, the most important applications, i.e., small signal analysis via mode estimation and DN dynamic equivalencing, are briefly discussed.

3.1. Mode Estimation

The dynamic response of a system, subject to small perturbations, can be approximated by a sum of N damped sinusoidal functions:

$$\hat{y}(t) = \sum_{i=1}^{N} A_i e^{\sigma_i t} \cos(\omega_i t + \varphi_i) + e(t), i = 1 \dots N \tag{8}$$

where $\hat{y}(t)$ is the estimated response and ω_i, σ_i, A_i and ϕ_i is the system mode angular frequency, damping factor, amplitude and phase [10,12]. Measurement-based small-signal analysis involves the identification of modal parameters, i.e., ω_i and σ_i, by analyzing system responses. In the framework of ACTIVATE, measurement-based modal analysis is performed by means of ARMAX modeling as follows [10]:

- **Step 1**: The available signals (dynamic responses) are sampled at a fixed rate allowing the use of z-transform as follows:

$$\hat{Y}(z) = \frac{B(z)}{A(z)} U(z) + \frac{C(z)}{A(z)} e(z) \tag{9}$$

where $B(z)$ and $A(z)$ constitute the transfer function $H(z)$ of the system and $e(z)$ is the unknown input of the system, e.g., noise. The polynomials of (9) are defined as

$$A(z) = 1 + \sum_{\ell=1}^{p_a} a_\ell z^{-\ell} \tag{10}$$

$$B(z) = \sum_{\ell=1}^{p_b} b_\ell z^{-\ell} \tag{11}$$

$$C(z) = \sum_{\ell=1}^{p_c} c_\ell z^{-\ell}. \tag{12}$$

Here, a_ℓ, b_ℓ and c_ℓ are the parameters of the autoregressive model, the exogenous inputs and the moving average model of order p_a, p_b and p_c, respectively. The optimal model order is determined via an iterative process until a pre-defined tolerance ΔR_h^2 between two successive steps h and $h-1$ is achieved [10]. This way, only the dominant system modes are included in (9). The coefficient of determination R^2 at step h is defined as

$$R_h{}^2 = \left(1 - \frac{\sum_{k=1}^{K}(y_h[k] - \hat{y}_h[k])^2}{\sum_{k=1}^{K}(y_h[k] - \bar{y}_h)^2}\right) \cdot 100. \tag{13}$$

where $\bar{y}$ is the mean value of the measured signal y.

- **Step 2**: Screening of the derived mode estimates is applied to exclude possible artificial components. As such, we can consider modes with frequencies outside the range of 0.05 Hz to 3 Hz [22] and/or having a damping factor higher than, for example, 10 s^{-1}.
- **Step 3**: If signals from several system buses are available, multi-signal analysis is performed via k-medoids clustering, considering as inputs the mode frequency, damping factor and normalized energy, the latter being defined for the i-th mode (here, $i = 1, \ldots, W$) as

$$\bar{E}_i = \frac{(\omega_i A_i)^2}{\sum_{i=1}^{W}(\omega_i A_i)^2}. \tag{14}$$

- **Step 4**: A two-step mode classification procedure is applied. Initially, modes are classified in terms of mode frequency, i.e., low (below 1 Hz) and high frequency (above 1 Hz) oscillatory modes [22]. At the second level, modes are distinguished as poorly or well damped. The mode with the lowest damping factor is characterized as the critical system mode and is used as a indicator of the overall system small-signal stability.

3.2. DN Dynamic Equivalent Modelling

DEMs describe the aggregated real and reactive power response of a system bus following a voltage disturbance. This way, DSOs can derive reduced, equivalent models of their own networks and couple them to the TN model for use by the TSO. The concept and the structure of the proposed DEM is depicted in Figure 6. The adopted equivalent model has the form of (15)–(19) [10]

$$y(t) = y_t(t) + y_r(t) \tag{15}$$

$$y_r(t) = L^{-1}[g_2(t)G(s)] \tag{16}$$

$$y_t(t) = y_0[\lambda_1\left(\frac{V(t)}{V_0}\right) + \lambda_2] \tag{17}$$

$$y_s(t) = y_0\left[\kappa_1\left(\frac{V(t)}{V_0}\right) + \kappa_2\right] \tag{18}$$

$$G(s) = \frac{b'_0 + b'_1 s + \ldots + b'_{p'_s} s^{p'_s}}{\alpha'_0 + \alpha'_1 s + \ldots + \alpha'_{p_a} s^{p'_a}}. \tag{19}$$

Here, $y(t)$ denotes either the real or the reactive power response and $G(s)$ is the corresponding transfer function with parameters b'_i of order p'_s and α'_i of order p'_a. The real/reactive power model parameters are calculated via ARMAX modeling by using a

voltage disturbance response as input and the power response as output, respectively. Coefficients λ_1, λ_2 and κ_1, κ_2 are determined from the overshoot and the new steady-state points, respectively. The optimal order of $G(s)$ is determined similarly to Step 1 of mode estimation [10].

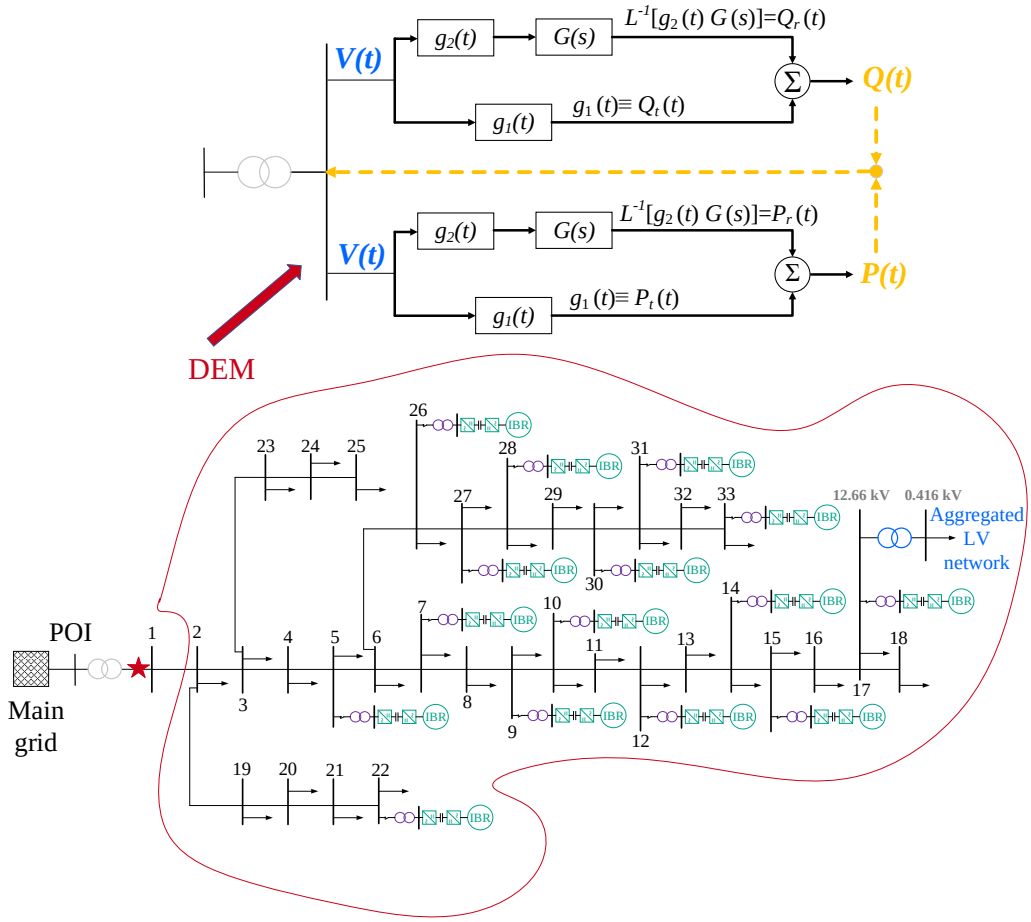

Figure 6. Detailed DN (**down**) and its DEM (**up**).

4. Simulation Model

4.1. T&D Network

For the evaluation of the performance of the designed AS and the dynamic analysis applications simulations are conducted using the T&D network of Figure 7. The T&D power system consists of a high voltage (HV) TN, as well as of a primary medium voltage (MV) and a secondary low voltage (LV) DN. The TN and primary and secondary DNs are modified versions of the IEEE 39 Bus Test System [23], the 12.66 kV IEEE 33 Bus Test System [24] and the unbalanced three-phase IEEE European LV test feeder [25], respectively.

4.2. Quasi-Static Modelling

Quasi-static simulations for two indicative days, i.e., a sunny day and a cloudy day, are performed in the OpenDSS [26] software v961.1 to assess the performance of the AS framework. In this series of simulations, the TN is modeled as an infinite feeder. In the modified primary DN, 15 PVs and 20 BES are considered. Accordingly, in the secondary DN, 32 PV/BES units are added. The POI and capacity of the PVs at the primary and the secondary DN are summarized in Table 1.

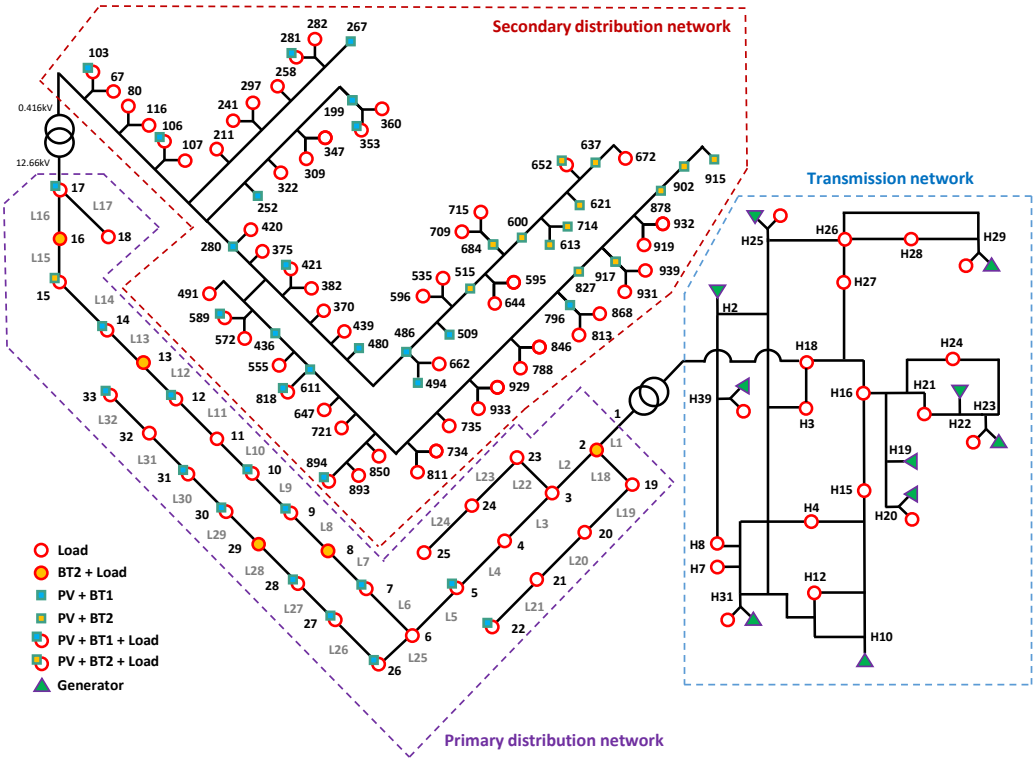

Figure 7. Topology of the T&D network.

All loads were modeled by using 1 min timeseries. In particular, the primary DN load profiles are daily electricity timeseries from the [27] dataset with 1 h resolution. By applying linear interpolation, the corresponding 1 min profiles are derived and are randomly sited at the primary DN buses. In general, the rated active power and power factor (PF) of each load are similar to those of [24]. For the secondary DN, the real power profiles of [25] are adopted with a PF 0.95 lagging (all loads are single-phase). Regarding PVs, 24-h sunny and cloudy generation profiles with 1 min resolution are used [28]. The nominal PF of PV/BES at the primary and secondary DN is 0.9 and 0.85, respectively. Considering BES, two types are used, namely BT1 and BT2:

- BT1: are only equipped with PS capabilities, assuming an initial SoC = 50%,
- BT2: provide VR, VUM and PS ASs, assuming an initial SoC = 30% and 10% during a cloudy and a sunny day, respectively.

The POI and capacity of BT1 and BT2 BES are presented in Table 2. The minimum, $SOC_{\min}$, and maximum, $SOC_{\max}$, is 0.1 and 0.9, respectively. BESs are modeled in terms of their energy content (E) via

$$E(t) = E(t-1) + \eta_c \cdot P_c(t) \cdot \Delta t - \frac{1}{\eta_d} \cdot P_d(t) \cdot \Delta t \tag{20}$$

where Δt is the time step taken equal to 1 s, and P_c and P_d are the BES charging and discharging power, respectively; η_c and η_d are the corresponding charging/discharging BES efficiency taken equal to 0.95. Considering PS, it is assumed that $k = 2$, $RR_{\min} = -4$ W/s and $RR_{\max} = +4$ W/s. Finally, the proposed VR, VUM, CM and PS are implemented in MATLAB R2022b.

Table 1. PV installed capacity.

Primary DN		Secondary DN	
Node	**kWp**	**Node**	**kWp**
5, 14, 31, 33	350	103, 199, 267, 280, 281, 421, 436, 480, 486, 515, 589, 600, 613, 621, 652, 684, 796, 818, 878, 894, 902, 917	7.5
7, 22	500		
9, 12, 15, 27	700		
10, 17	300		
26, 28	250	106, 252, 353, 494, 509, 611, 637, 714, 827, 915	15
30	800		

Table 2. BES installed capacity.

BT1			
	Node	**kWh**	**kW**
Primary DN	5, 14, 31, 33	35	100
	7, 22	50	145
	9, 12, 15, 27	70	200
	10, 17	30	85
	26, 28	25	70
	30	80	230
Secondary DN	106, 252, 353, 494, 509, 611	1.5	2.15
	103, 280, 199, 267, 281, 421, 436, 480, 486, 589, 818, 796, 894	0.75	4.35

BT2					
Primary DN			**Secondary DN**		
Node	**kWh**	**kW**	**Node**	**kWh**	**kW**
2	1000	500	515, 714, 878	10	5
8	500	250	600, 613, 621	22.5	7.5
13	450	225	652, 684	30	7.5
15	250	220	902	15	7.5
16	550	275	915	25	12.5
29	600	300	637	45	15
			827	5	5
			917	5	2.5

4.3. Power System Dynamics Modelling

The dynamic analysis tools are tested via dynamic simulations in PowerFactory–DIgSILENT [29]. In this case, the TN is modeled in detail and consists of 32 transmission lines, 12 transformers, 19 constant power (CP) loads and 10 synchronous generators (SGs) equipped with IEEE type-1 exciters [23]. Considering the DN model, all IBRs (PV and BES units) are assumed connected to the grid via full scale power converters modeled as type 4A [30] and operate under a constant power ($P-Q$) mode. The primary and secondary DN loads are represented also as CP. In all test cases, a tolerance $\Delta R_h^2 = 1\%$ is considered to ensure high accuracy in the parameter estimates as well as minimal (optimal) model order, i.e., either regarding the mode estimates or the $G(s)$ parameters of DEM.

5. Quasi-Static Simulation Results

In this section, the performance of the designed AS is evaluated by conducting quasi-static simulations by using the T&D network of Figure 7.

5.1. Quasi-Static Simulation

Two scenarios are examined, assessing the effectiveness of the ASs:

- Scenario 1: VR, VUM and PS are examined
  - Sunny day: in the primary DN VR is provided by the DRES/BT2 units. In the secondary DN, both VUM and VR issues are solved by the DRES/BT2 units; BT1 units remain idle.
  - Cloudy day: in the primary DN PS and VR are provided by the DRES/BT2 units. In the secondary DN, PS, VUM and VR issues are solved by the DRES/BT2 units. In both the primary and secondary DNs BT1 units are used to provide only PS AS.
- Scenario 2: VR, VUM, PS and CM are examined
  - Cloudy day: in the primary DN PS, VR and CM is attributed to DRES/BT2 units and PS to BT1 units. For the secondary DN the same assumptions as in Scenario 1 apply.

In both scenarios, the permissible voltage range for the primary DN is within 0.95–1.05 pu and for the secondary DN 0.9–1.1 pu.

5.1.1. Scenario 1

Indicative rms positive-sequence voltage profiles of the primary and the secondary DN buses 17 and 652, respectively, are presented in Figure 8. Results are depicted separately for the cloudy and the sunny days, i.e., Figure 8a,b. It can be seen that by using the proposed VR scheme the voltage levels are successfully maintained within the prescribed voltage limits for both DNs. Comparing Figure 8a and Figure 8b, it can be realized that overvoltages are more prone to occur during a sunny day than during a cloudy day, starting at 10:08 and last up to 17:27. The same remarks can be also deduced by analyzing the voltage profiles of all DN buses.

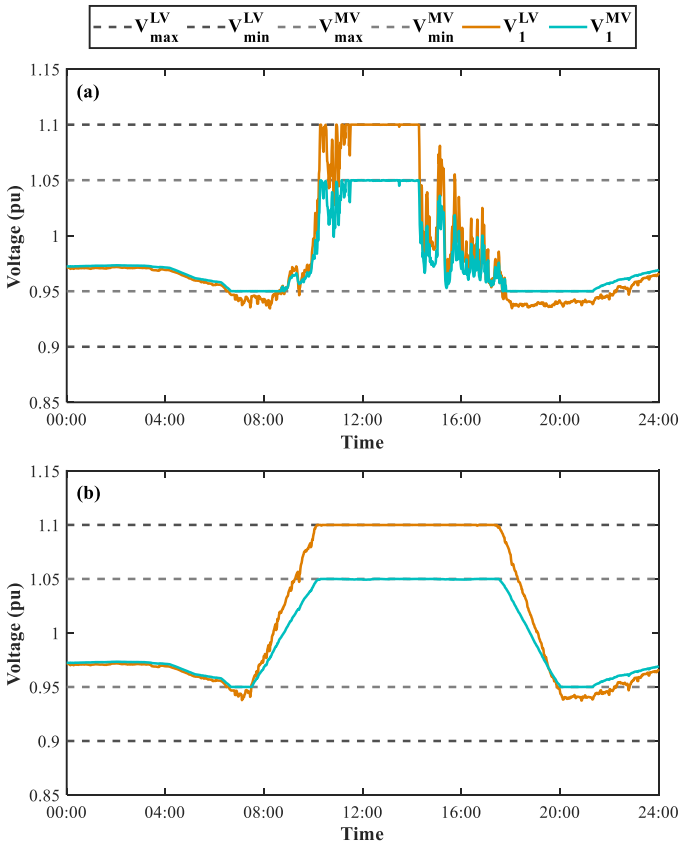

Figure 8. Positive-sequence voltage profiles of a primary and a secondary DN bus for the (**a**) cloudy and (**b**) sunny day.

The efficiency of the VUM AS is investigated in Figure 9 by means of cumulative distribution function plots of the zero- (VUF0) and the negative-sequence (VUF2) voltage unbalance factors. VUF0 and VUF2 are defined as the ratio of the zero-, negative-voltage to the corresponding positive-sequence voltage component. The cumulative distribution functions are derived by analyzing the rms voltages of all secondary DN buses and refer to the cloudy day case; similar cumulative distribution functions are also derived for the sunny day. The VUF0 (Figure 9a) and VUF2 (Figure 9b) results are evaluated by assuming VUM ON and OFF. It can be seen that by absorbing zero- and negative- sequence currents in terms of the proposed scheme the voltage asymmetries are reduced (VUF0 is below 2% and VUF2 below 0.8%). This is achieved by compensating locally the zero- and negative-sequence currents, thus reducing the corresponding voltage sequence drop along the lines and eventually mitigating the bus voltage asymmetries, in particular, absorbing the zero-sequence current results into a neutral point shift toward zero and consequently to the mitigation of the zero-sequence voltage asymmetry [31]. For VUM OFF, VUF0 can reach 6%, while VUF2 is below 1.2%. It should be indicated that for VUF2, a limit of 2% is prescribed by the IEEE 1547 Std. [32].

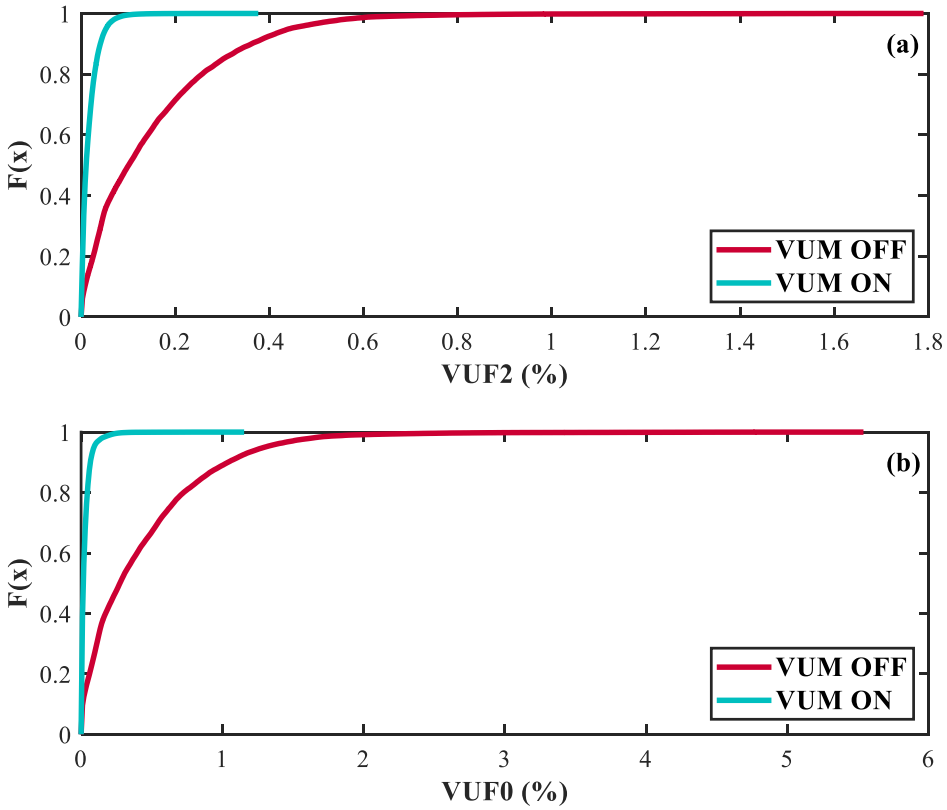

Figure 9. Cumulative distribution function of (**a**) VUF2 and (**b**) VUF0.

The effectiveness of the adopted PS algorithm is evaluated in Figure 10a. Indicatively, the daily active power profiles of BT1 at bus 15 are compared, assuming that the PS control scheme is ON and OFF. Results are presented for the cloudy day (extreme fluctuations). Despite the strong fluctuations, smoother profiles are derived by applying the RRL PS algorithm, as the control response is in line with the pre-defined ramp-rate limits ($RR_{\min} = RR_{\max} = 4$ W/s). The corresponding SoC profile of the BES is plotted in Figure 10b with regard to $SoC_{ref} = 50\%$. It can be seen that the SoC varies within 10% to 60% with an average value of $\overline{SoC} = 50\%$. Despite the unequal energy absorbed during the ramp-up and ramp-down, the adopted recovery mechanism supervises the SoC and ensures that at the end of the PS period (approximately at 18:00), it remains equal to $SoC_{ref} = 50\%$. This is an important feature that ensures the availability of the BES units to

provide or store sufficient energy in order to support AS during the next day [15]. Similar results have also been derived for the rest of the BT1 units.

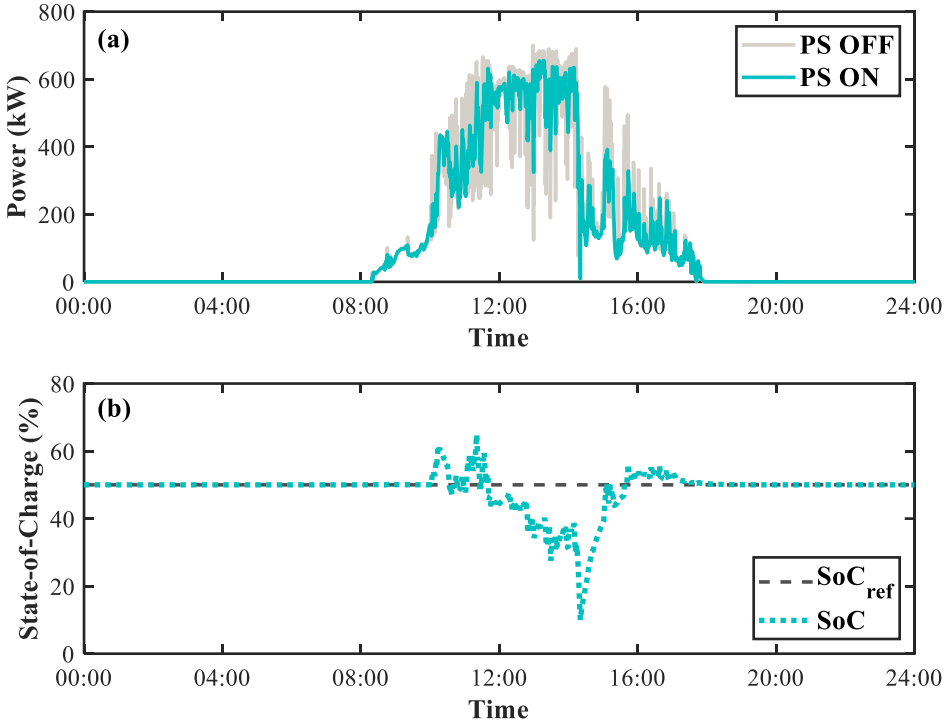

Figure 10. (**a**) Daily PV output power profile during a cloudy day. (**b**) Daily *SoC* profile of BT1–15.

The overall AS system performance is evaluated by analyzing the total reactive and active power exchanged by the DRES and the BES units at the primary and secondary DN. In particular, in the bar graphs of Figure 11 the total reactive energy absorbed/injected by the DRES (E^{Q}_{DRES}) and the BES (E^{Q}_{BES}) units is analyzed for the cloudy and the sunny day. Note that a plus sign denotes reactive power absorption and a minus sign injection. The corresponding active power is analyzed in Table 3 per AS usage, i.e., for VS or PS. It should be reiterated that for VUM, reactive power is exclusively used. From the results, the following remarks can be generally inferred:

- Comparing the cloudy and sunny day:
  - Considering the cloudy day significantly higher amounts of energy are used for PS compared to VR. This is because of the excessive primary source (PV) fluctuations and their pronounced effect compared to network overvoltages.
  - Considering the sunny day, due to the higher PV generation and the inherently smoothed sun irradiation, PS descends and VR becomes important; thus, high amounts of active and reactive power are absorbed to resolve the resulting overvoltage issues.
- Primary and secondary DNs:
  - Significant amounts of reactive power are used in the primary DN to solve overvoltage problems. Such issues are of less importance in the secondary DN for the examined case.
  - Due to primary DN stiffness higher amounts of reactive power are required for VR. This is also attributed to the higher X/R ratio of the distribution lines.
  - accordingly, for VR at the secondary DN more active power is absorbed by the BES units than those of the primary DN.

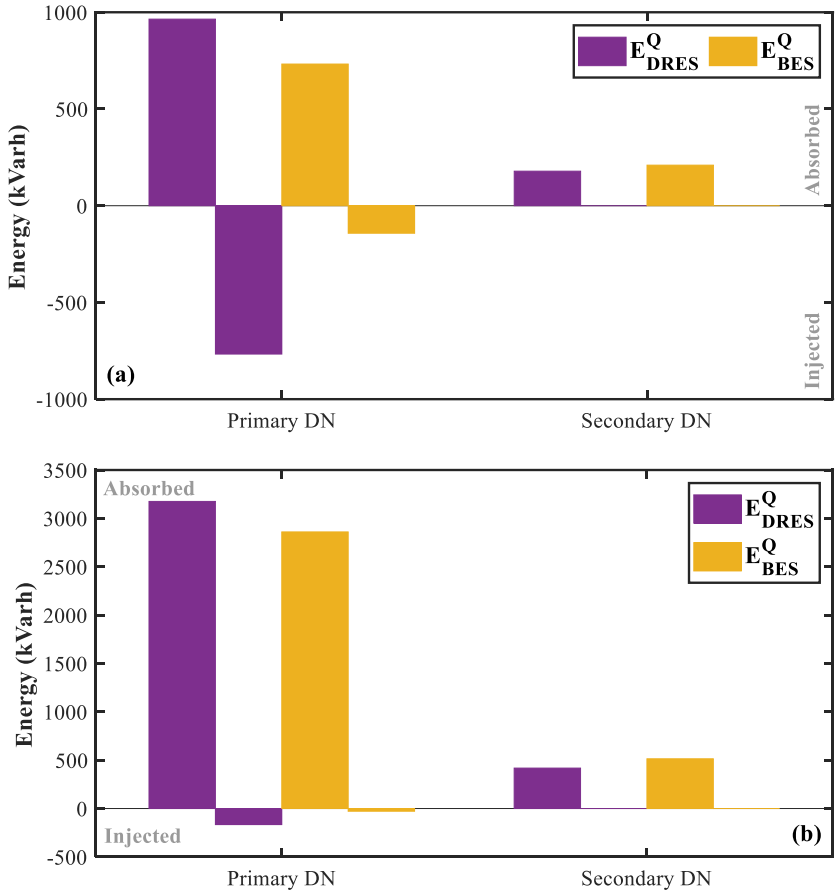

Figure 11. Total absorbed/injected energy related to reactive power by DRES/BESs units during (**a**) a cloudy and (**b**) a sunny day.

Table 3. Total absorbed/injected energy by BESs.

Day	Network	AS	E^{P}_{BES} (kWh)	
Cloudy	Primary DN	VR	Absorbed	-
			Injected	-
		PS	Absorbed	1756.93
			Injected	1585.63
	Secondary DN	VR	Absorbed	17.56
			Injected	-
		PS	Absorbed	77.95
			Injected	70.35
Sunny	Primary DN	VR	Absorbed	91.18
			Injected	-
		PS	Absorbed	-
			Injected	-
	Secondary DN	VR	Absorbed	139.16
			Injected	-
		PS	Absorbed	-
			Injected	-

5.1.2. Scenario 2

For Scenario 2 CM analysis is also performed. The cable ampacity is provided in Table 4.

Indicative current profiles flowing in the primary DN cables L4 and L5 are compared in Figure 12, assuming that the CM scheme is ON and OFF. The corresponding cable ampacity is also indicated in the figures (flat line). The DRES/BES units at bus 5, 7, 26, 27 inject reactive power according to the proposed CM method. This entails that the current of

the cables is restored within the permissible limits, and consequently the cable overloading is alleviated. The reactive energy absorbed/injected by the DRES and the BES participating in the proposed VR and CM schemes is summarized in Figure 13. The injected reactive power by DRES units at bus 5, 7, 26, 27 is indicated by the minus sign. This reactive power injection results into new overvoltage events. Nevertheless, in the frame of the holistic AS framework apart from eliminating the cables overload, the network voltages must be also maintained within the stipulated limits. Therefore, the DRES and BES units at bus 12, 14, 15 and 17 that participate in the VR scheme re-adjust their reactive power set points (additional reactive power absorption) and eventually regulate all network voltages. The additional reactive power absorption can be realized by comparing the results of Figure 13 for the cases of CM ON and OFF.

Table 4. Primary DN cable data.

Cable No.	*R*/*X*	Ampacity (A)
L1–L4, L25, L26, L29	1.96	205
L5, L14, L19, L27, L28	1.25	195
L6	0.30	150
L7, L10, L11	3.02	150
L8, L9, L15, L22	1.40	150
L12, L17, L23, L24	1.27	115
L13, L16, L21	0.75	115
L18, L30	1.02	70
L20, L31	0.85	70
L32	0.65	70

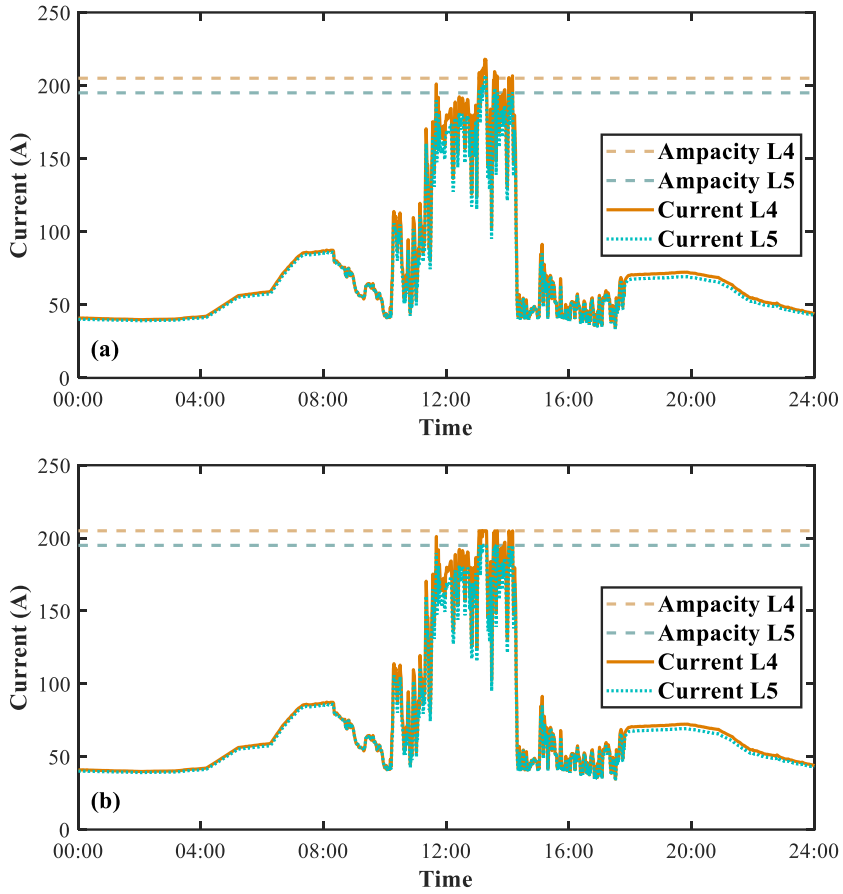

Figure 12. Current profiles of two indicative primary DN lines (**a**) CM OFF and (**b**) CM ON.

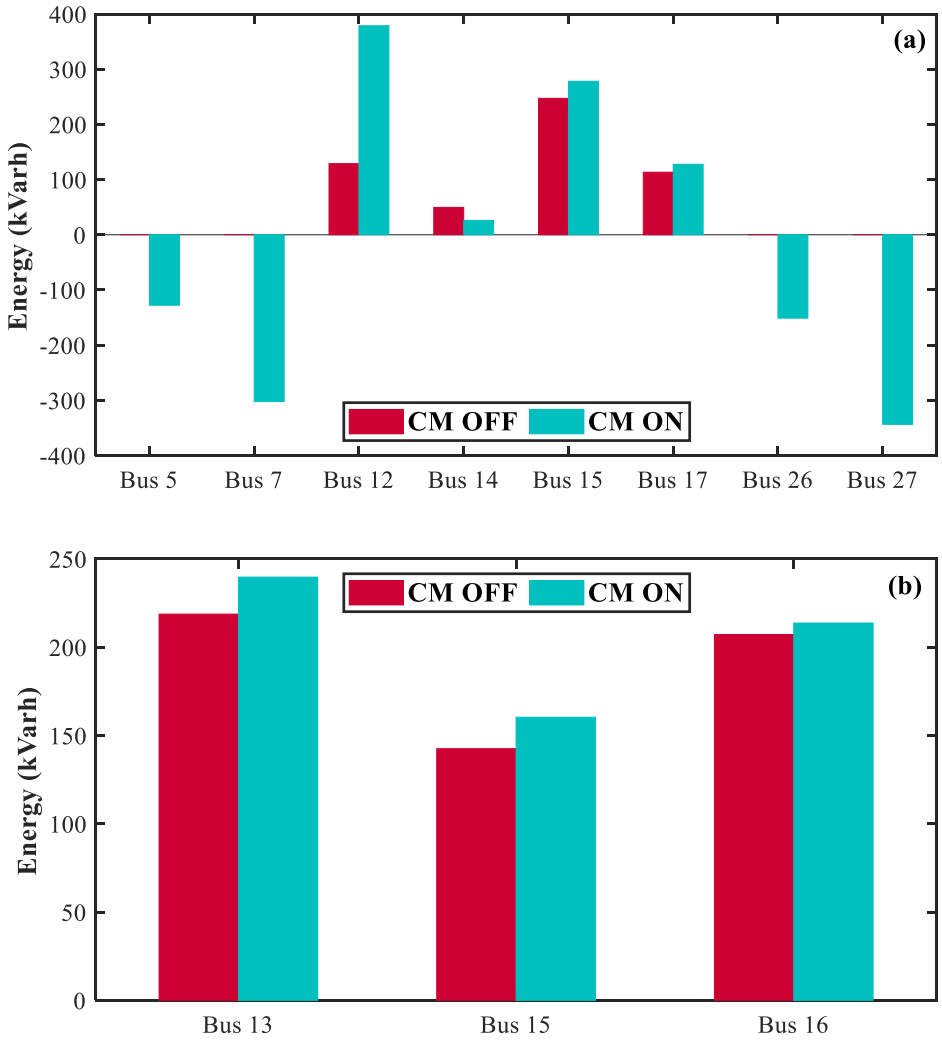

Figure 13. Comparison of reactive power usage of (**a**) DRES and (**b**) BES units situated at the primary DN assuming CM ON and OFF.

Finally, to analyze and evaluate the total injected and absorbed reactive power of the DRES/BES units situated at the primary DN, the results are presented in Figure 14a and in Figure 14b, respectively. Comparison of the bar graphs in Figure 14a for the CM ON and OFF cases reveals that the injected reactive energy increases in DRES due to the activation of the CM algorithm. On the other hand, Figure 14b comparisons show that the activation of the CM leads to a slight increase in the energy absorbed by the DRES and BES. This is attributed to the additional reactive power required to tackle the overvoltage issues described above as a result of the reactive power injection into the network by the DRES units at bus 5, 7, 26, 27 to alleviate cable overloads.

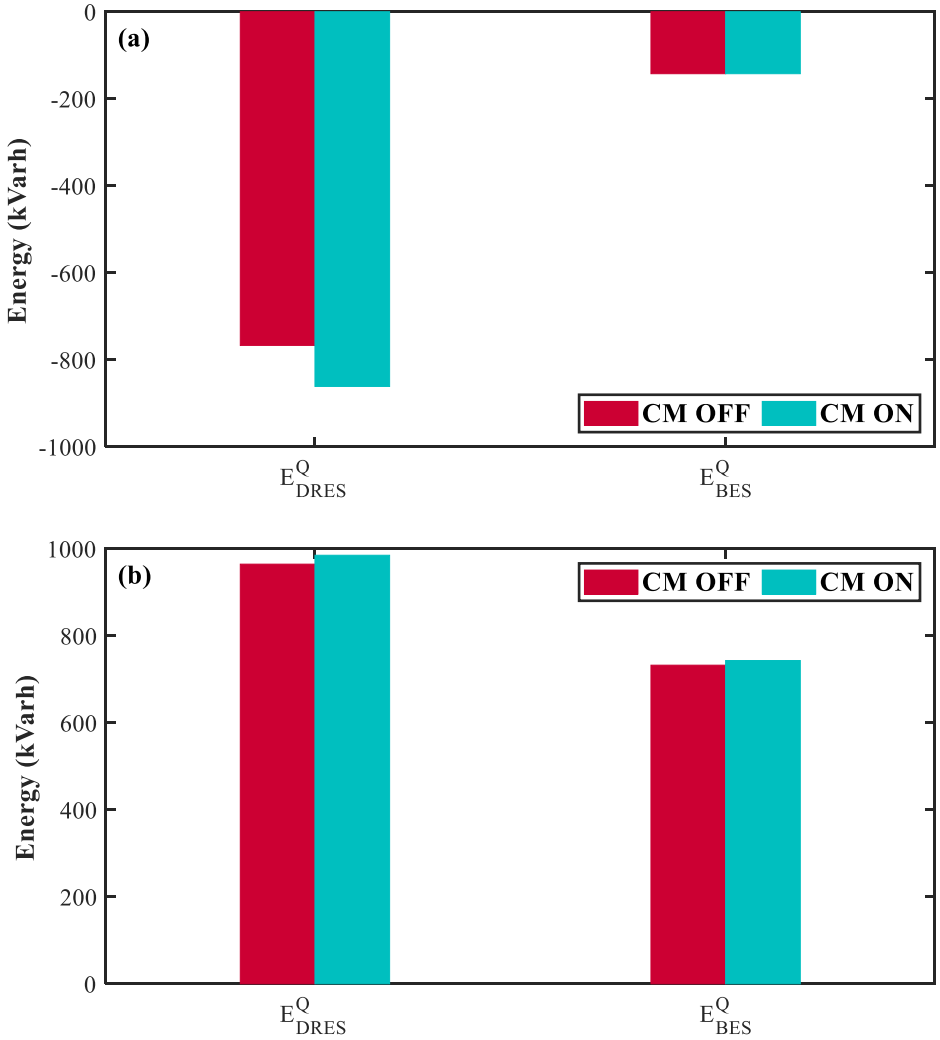

Figure 14. Total (**a**) absorbed and (**b**) injected reactive power of DRES/BES units situated at the primary DN assuming CM ON and OFF.

6. Dynamic Simulation Results

The performance of the DEM is demonstrated by using time-domain simulations. The DN is excited by a 5% step-down voltage disturbance via tap-changing the HV/MV transformer. Note that the initialization of the dynamic simulations model relies on the quasi-static analysis described above. This is achieved by the concurrent use of the OpenDSS [26] and DIgSILENT Power Factory [29] software tools. In particular, the pre-disturbance operating conditions in DIgSILENT are those resulted by the application of the proposed AS in Scenario 1 at a specific time instant of the sunny day, i.e., t = 13:40 (time instant corresponding to the highest DRES generation).

6.1. DN Dynamic Equivalencing

In Figure 15, the estimated (ARMAX modeling) and the original (simulated by DIgSILENT model) real and reactive power dynamic responses at bus 1 of the primary DN are compared. Note that, in the DIgSILENT model and accordingly in the figures, a negative sign denotes power flow from the TN to the DN. The R^2 for both the real and the reactive power responses is higher than 99%, thus the proposed ARMAX model can accurately represent the DN dynamics. By analyzing the responses, it can be seen that after the step in the voltage disturbance the DN behaves as an impedance and consequently both the real and the reactive power change immediately after the voltage step-down. Afterwards, the dynamics of the DN, i.e., loads and IBRs tend to restore the DN power, at least to a

certain extent. This recovery is approximately of exponential form and might be oscillatory depending on the DN mixture. Note that the overshoot and the new steady state are related non-linearly to the voltage response [33].

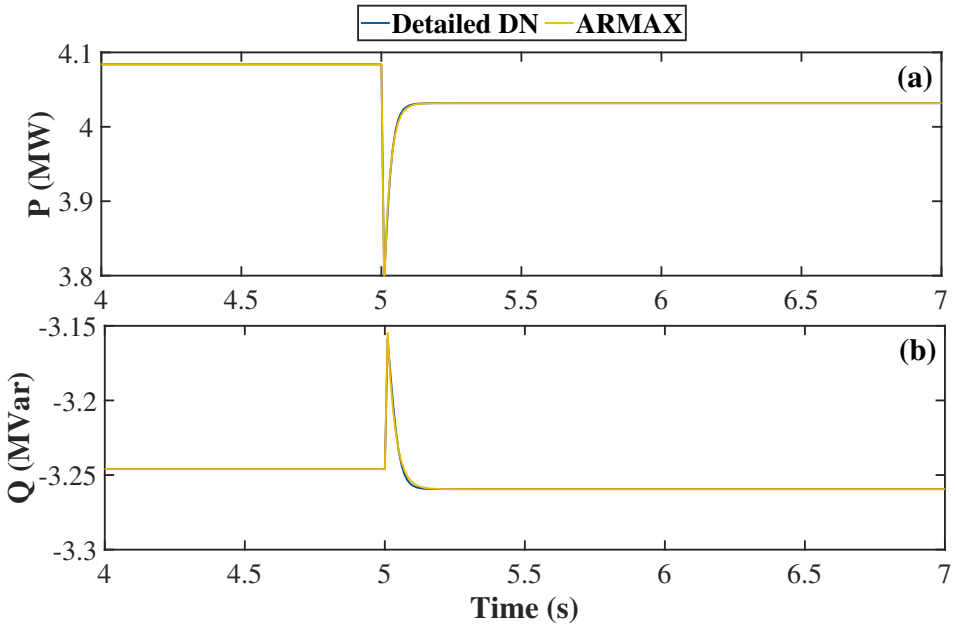

Figure 15. Dynamic responses of the DN (**a**) real and (**b**) reactive power modeling.

6.2. Effect of IBRs and Load Modelling

To investigate further the DN dynamics and more explicitly the effect of IBRs and load modeling, the system loads of the primary DN are also represented as exponential (EXP) and constant impedance (CZ). The real P_{EXP} and reactive P_{EXP} power of the EXP model is described by

$$P_{EXP} = P_0 \left(\frac{V}{V_0} \right)^{n_P} \tag{21}$$

$$Q_{EXP} = Q_0 \left(\frac{V}{V_0} \right)^{n_Q} \tag{22}$$

where V is the network voltage, V_0 is the pre-disturbance voltage magnitude and P_0 and Q_0 the corresponding pre-disturbance real and reactive power, respectively. For the EXP model, universal parameters are selected, i.e., $n_P = 0.74$ and $n_Q = 1.3$, according to [34]. The CZ model results by substituting $n_P = 2$ and $n_Q = 2$ into (21) and (22), respectively.

In Figure 16, the real and reactive power dynamic responses of bus 1 of the primary DN are summarized by using the different load models. Results are compared for the following cases of IBR penetration:

- Low IBR penetration: DRES/BES are hosted at buses 5, 7, 9 and 10 of the primary DN. Results are presented in Figure 16a,d.
- Moderate IBR penetration: DRES/BES are hosted at buses 5, 7, 9, 10, 12, 14, 15, 17 and 22 of the primary DN. Results are presented in Figure 16b,e.
- High IBR penetration: all primary DN DRES/BES units described in Tables 1 and 2 are used. Results are presented in Figure 16c,f.

The comparison of the results reveals the effect of IBR penetration and load modeling on the steady state and the transient response. In particular, as the IBR penetration increases, the DN real power prior to the disturbance tends to zero and becomes positive for high IBR penetration and all load models; this case is characterized by an excess of IBR generation (compared to local demand), and thus, reverse power flow from the DN to the TN occurs. The steady state real and reactive power after the disturbance depends on the adopted load

model. This can be elucidated by assuming that the aggregated real and reactive power of the IBR and load prior to the disturbance is P_{IBR}, Q_{IBR} and P_{Load}, Q_{Load}, respectively, and thus

$$P_{DN} = P_{IBR} - P_{Load} \tag{23}$$

$$Q_{DN} = Q_{IBR} - Q_{Load} \tag{24}$$

is the corresponding real and reactive power at bus 1 for voltage V_0. After the step-down disturbance, the new steady-state voltage is V' and the corresponding real and reactive power values are P'_{DN}, P'_{IBR} and P'_{Load} as well as Q'_{DN}, Q'_{IBR} and Q'_{Load}, respectively. Due to the $P-Q$ control mode of the IBR $P'_{IBR} = P_{IBR}$ and $Q'_{IBR} = Q_{IBR}$. For $V' < V$ the CZ and the EXP model load power becomes $P_{Load} > P'_{Load}$ and $Q_{Load} > Q'_{Load}$; thus, from (23) and (24) it occurs that the real and reactive power prior to and after the disturbance yield $P_{DN} < P'_{DN}$ and $Q_{DN} < Q'_{DN}$, respectively. On the contrary, for the CP model $P_{Load} = P'_{Load}$ and $Q_{Load} = Q'_{Load}$, and thus $P_{DN} \approx P'_{DN}$ and $Q_{DN} \approx Q'_{DN}$ (small differences between the two steady states are due to losses across the DN lines).

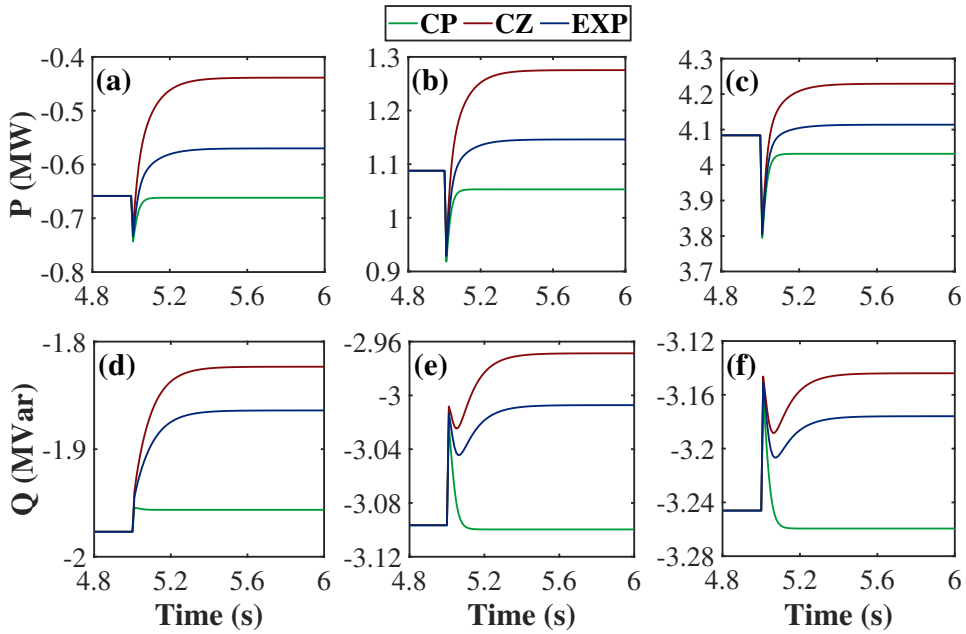

Figure 16. Dynamic responses for low IBR penetration of the (**a**) real and (**d**) reactive power, for moderate IBR penetration of the (**b**) real and (**e**) reactive power and for high IBR penetration of the (**c**) real and (**f**) reactive power.

Considering the DN dynamics, they become more complex with increasing IBR penetration. This is more pronounced for the reactive power response, where an oscillatory behavior is observed for moderate and high IBR penetration by using the CZ and the EXP models. Regarding real power, it can be observed that as the IBR penetration increases, the transient overshoot becomes higher for all load models. The differences in the dynamic responses by using the different load models can be quantified by comparing the corresponding settling time in Table 5. It is evident that the CP modeling approach results into faster and more steep responses compared to the CZ and the EXP models. This also complies with the fact that CP models yield the most pessimistic results from a stability perspective [35].

Table 5. Settling time for the different load models and varying IBR penetration.

Case	Load Model	Real Power	Reactive Power
Low IBR penetration	CP	0.0819 s	0.1011 s
	CZ	0.3216 s	0.3516 s
	EXP	0.3042 s	0.3707 s
Moderate IBR penetration	CP	0.0817 s	0.0948 s
	CZ	0.3053 s	0.4218 s
	EXP	0.2769 s	0.4486 s
High IBR penetration	CP	0.0806 s	0.0931 s
	CZ	0.2768 s	0.4373 s
	EXP	0.2299 s	0.4594 s

6.3. Mirroring the DN in Dynamic Simulations

For demonstration purposes, a case study is considered, where the detailed DN is replaced by the developed ARMAX DEM and is integrated into the T&D network model to directly interact with the TN. In Figure 17, the ARMAX DEM developed within PowerFactory is presented by means of a block structure diagram. As shown, the DEM is a dynamic model (illustrated also in Figure 6) that can represent as a block diagram the two nonlinear functions and the linear transfer function of (9)–(12) [33]; in practice, the DEM represents the internal system, i.e., the DN state in real time. This dynamic model receives as input the voltage measurement at the secondary side of the HV/MV transformer and provides as output the total power (real and reactive) for the overall DN. The external system (main grid) pertains to the TN of Figure 7. Indicative real and reactive power responses of the detailed DN and its DEM are presented in Figure 18, considering a voltage step-down disturbance equal to 5%. Comparing the DEM responses with the original ones, the accuracy and reliability of the developed model are verified as R^2 for the real and reactive power higher than 99%.

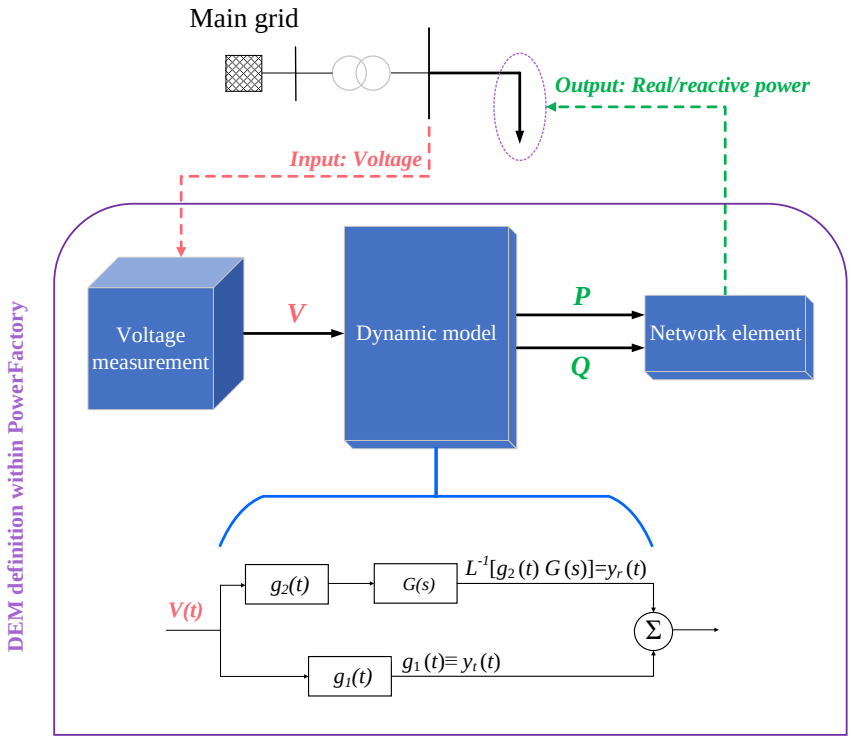

Figure 17. DEM integration in DIgSILENT Power Factory.

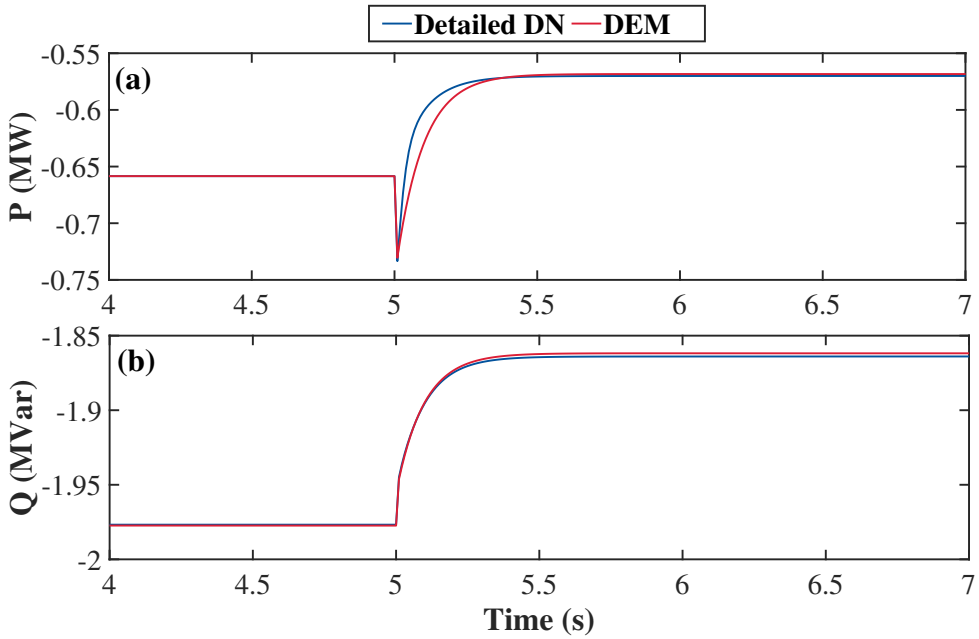

Figure 18. DEM results for low IBR penetration. (**a**) Real and (**b**) reactive power modeling.

7. PHIL Testing

The performance of the proposed mode estimation technique is evaluated in a PHIL simulation environment. To create the PHIL setup, a HV TN and two MV primary DNs are implemented on a digital real-time simulator. Additionally, a secondary LV DN is designed using the laboratory infrastructure of the Dynamic Power System Laboratory of the University of the Strathclyde (ACTIVATE project partners). The TN is a modified version of the well-known Kundur Two Area Power System model [36]; primary DNs are designed by applying topological modifications on the benchmark European MV grid of CIGRE [37]. The topology of the examined setup is described in detail in [38].

To analyze the dynamic behavior of the examined setup, nine PMUs are used, located at the different levels of the power system. In particular, an adaptive filter-based PMU is installed at the secondary DN and eight P class PMUs are simulated using the GTNET-PMU firmware of the digital real time simulator [38]. Three of the virtual PMUs are located at primary DN buses, and five of them at TN buses. Further details concerning the sitting and the characteristics of the PMUs can be found in [38].

To evaluate the proposed mode estimation technique, a ringdown event is generated by connecting and disconnecting a load at the TN. The event under study is the first event of Set-1 (for further details see Section II.B of [38]). During the ringdown, voltage responses are recorded using the PMUs. Recordings from all available PMUs are presented in Figure 19 alongside with the estimated responses, derived by ARMAX modeling. As shown, in all cases, a very good agreement between the recorded responses and the estimated ones is obtained, verifying that the proposed method captures accurately the dynamic behavior of the examined setup.

The inter-area mode parameters, resulted after the screening of the derived estimates, are illustrated in Figure 20. As shown, the analysis of individual signals/responses results in varying modal estimates (depicted as colorful dots in Figure 19), making it difficult for the system operator to identify the actual modal properties. This issue is resolved by adopting the proposed clustering approach. In this case, all modal parameters, resulted after the screening of the derived estimates, are grouped together, and a unique mode estimate is produced by means of clustering. This unique estimate is illustrated with a red star in Figure 20.

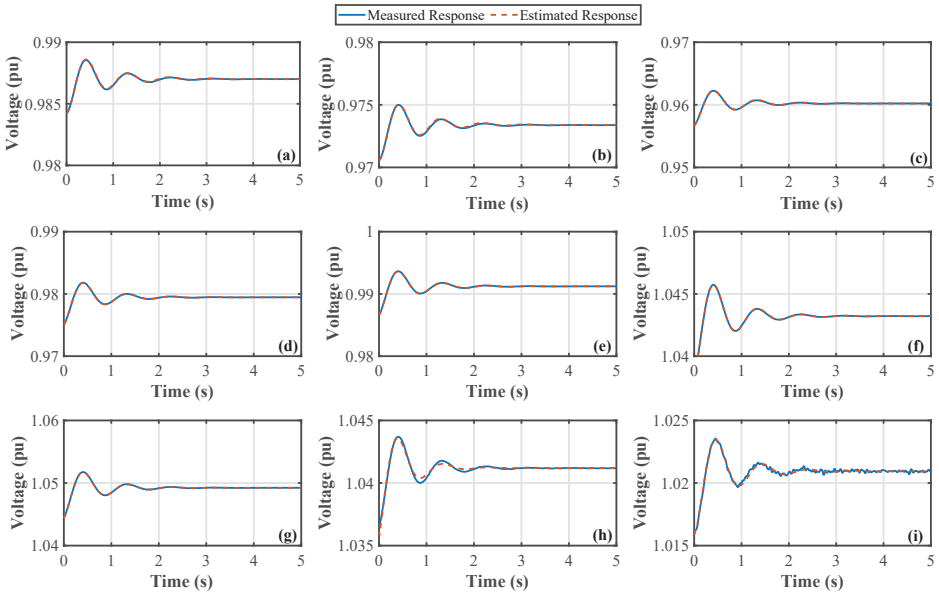

Figure 19. Voltage magnitude responses (in pu). Figure (**a**–**i**) refer to different PMUs, i.e., to different locations/buses of the examined setup. Further information concerning the exact location of the PMUs are provided in [38].

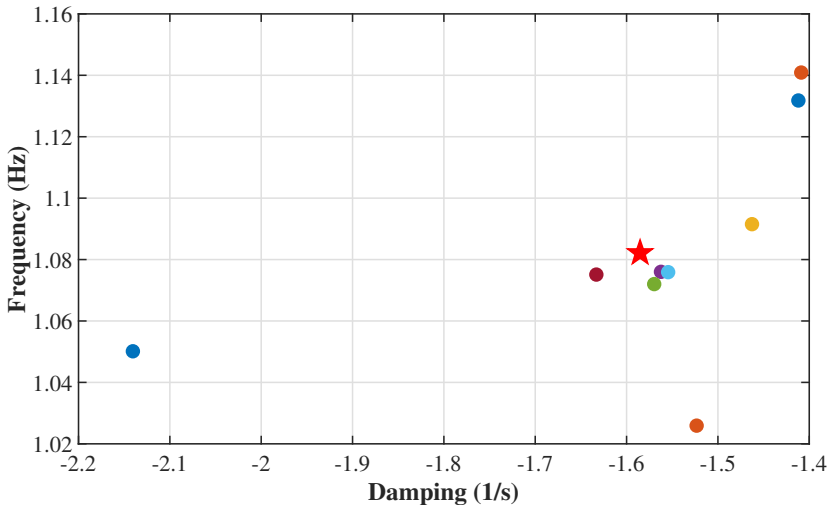

Figure 20. Identified modal parameters. Colorful dots denote modal estimates, resulted from single-signal analysis, i.e., by analyzing separately the available signals. The red star denotes the estimate resulted by the proposed multi-channel clustering-based approach.

8. Conclusions

In this paper, a comprehensive validation of a holistic system is presented. The proposed system consists of a set of hybrid control strategies to provide ASs (VR, VUM, PS with BES SoC recovery and CM) as well as a network monitoring system to support a number of online (small-signal stability analysis) and offline (DEM development) applications by exploiting measurements from different levels of the power system. The validation is performed by means of software and PHIL simulation results obtained in combined T&D network models. The following points are demonstrated:

- The proposed VUM, VR, PS and CM ASs can tackle holistically problems in both primary and secondary DNs under different operating conditions.
- The SoC recovery algorithm ensures the availability of BES units for the provision of PS ASs for the next day.

- The provision of the ASs depends on the weather conditions. This entails the different usage of the real and reactive power from DRES/BES units.
- Reactive power can be utilized to solve VR issues in primary DNs as well as in secondary DNs, despite the generally low X/R distribution line ratio of the latter.
- IBRs influence the transient response of DNs. The transient overshoot of the real and reactive power response increases with IBR penetration and generally the DN dynamics become faster (most importantly for the real power) and more oscillatory (more evident for the reactive power).
- Load modeling has a significant impact on the steady state after the disturbance and the transient response. In particular, the new steady state depends on the DN power recovery that is directly related to the load model. CP models result into faster recovery and smaller power variations prior to and after the disturbance. Accordingly, their transient responses are more steep and fast compared to CZ and EXP models.
- The developed DEM can accurately reproduce the dynamic response of the DN to external disturbances.
- The performance of the ARMAX mode estimation algorithm was successfully validated in the PHIL setup by using measurements at the three levels (transmission, primary and secondary distribution) of the power system.
- The results of the simulation and PHIL tests prove the consistency and the accuracy of the proposed AS and the dynamic response analysis tools, highlighting the adaptability to different power system configurations.

In summary, the proposed solution offers a holistic framework to provide ASs as well as to monitor and analyze different aspects of dynamic phenomena that may occur at the different parts of modern power systems. This concept can be used to improve the operation of TN and DN and enhance the reliability of the dynamic analysis of the corresponding power system operators as well as extending their visibility and coordination.

Author Contributions: Conceptualization, T.A.P., E.O.K. and G.C.K.; methodology, K.D.P., G.A.B.-N. and A.I.N.; validation, K.D.P., G.A.B.-N. and C.L.A.; writing—original draft preparation, T.A.P., G.C.K. and E.O.K.; writing—review and editing, G.C.K., A.I.N. and K.D.P.; All authors have read and agreed to the published version of the manuscript.

Funding: The research work was supported by the Hellenic Foundation for Research and Innovation (H.F.R.I.) under the "First Call for H.F.R.I. Research Projects to support Faculty members and Researchers and the procurement of high-cost research equipment grant" (Project Number: HFRI-FM17-229).

Data Availability Statement: Not applicable.

Conflicts of Interest: The authors declare no conflict of interest.

Abbreviations

The following abbreviations are used in this manuscript:

ARMAX	Autoregressive–moving average with exogenous inputs
AS	Ancillary Services
BES	Battery Energy Storage
CC	Central Controller
CP	Constant Power
CM	Congestion Management
CZ	Constant Impedance
DEM	Dynamic Equivalent Model
DN	Distribution Network
DRES	Distributed Renewable Energy Sources
DSO	Distribution System Operator
EXP	Exponential
IBR	Inverter Based Resources
LC	Local Controller

MPP	Maximum Power Point
PDC	Phasor Data Concentrator
PHIL	Power hardware-in-the-loop
PMU	Phasor Measurement Unit
POI	Point of Interconnection
PS	Power Smoothing
PV	Photovoltaic
RES	Renewable Energy Sources
RRL	Ramp-rate Limitation
SoC	State of Charge
TN	Transmission Network
TSO	Transmission System Operator
VR	Voltage Regulation
VUM	Voltage Unbalance Mitigation

References

1. Oureilidis, K.; Malamaki, K.-N.; Gallos, K.; Tsitsimelis, A.; Dikaiakos, C.; Gkavanoudis, S.; Cvetkovic, M.; Mauricio, J.M.; Maza Ortega, J.M.; Ramos, J.L.M.; et al. Ancillary Services Market Design in Distribution Networks: Review and Identification of Barriers. *Energies* **2020**, *13*, 917 . [CrossRef]
2. Kaushal, A.; Van Hertem, D. An Overview of Ancillary Services and HVDC Systems in European Context. *Energies* **2019**, *12*, 3481. [CrossRef]
3. Jay, D.; Swarup, K.S. A comprehensive survey on reactive power ancillary service markets. *Renew. Sustain. Energy Rev.* **2021**, *144*, 110967. [CrossRef]
4. Vatandoust, B.; Ahmadian, A.; Golkar, M.A.; Elkamel, A.; Almansoori, A.; Ghaljehei, M. Risk-Averse Optimal Bidding of Electric Vehicles and Energy Storage Aggregator in Day-Ahead Frequency Regulation Market. *IEEE Trans. Power Syst.* **2019**, *34*, 2036–2047. [CrossRef]
5. Ku, T.-T.; Lin, C.-H.; Hsu, C.-T.; Chen, C.-S.; Liao, Z.-Y.; Wang, S.-D.; Chen, F.-F. Enhancement of Power System Operation by Renewable Ancillary Service. *IEEE Trans. Ind. Appl.* **2020**, *56*, 6150–6157. [CrossRef]
6. Kotsampopoulos, P.; Hatziargyriou, N.; Bletterie, B.; Lauss, G. Review, analysis and recommendations on recent guidelines for the provision of ancillary services by Distributed Generation. In Proceedings of the 2013 IEEE International Workshop on Inteligent Energy Systems (IWIES), Vienna, Austria, 14 November 2013; pp. 185–190. [CrossRef]
7. Kryonidis, G.C.; Kontis, E.O.; Papadopoulos, T.A.; Pippi, K.D.; Nousdilis, A.I.; Barzegkar-Ntovom, G.A.; Boubaris, A.D.; Papanikolaou, N.P. Ancillary services in active distribution networks: A review of technological trends from operational and online analysis perspective. *Renew. Sustain. Energy Rev.* **2021**, *147*, 111198. [CrossRef]
8. *IEEE Std 1159-2019 (Revision of IEEE Std 1159-2009)*; IEEE Recommended Practice for Monitoring Electric Power Quality–Redline. IEEE, 2019; pp. 1–180. (*Place of Publication Not Identified*)
9. Kreeumporn, W.; Ngamroo, I. Integrated superconducting coil into PV generator for power smoothing and voltage regulation. In Proceedings of the 2015 IEEE International Conference on Applied Superconductivity and Electromagnetic Devices (ASEMD), Shanghai, China, 20–23 November 2015; pp. 159–160. [CrossRef]
10. Papadopoulos, T.A.; Kontis, E.O.; Barzegkar-Ntovom, G.A.; Papadopoulos, P.N. A Three-Level Distributed Architecture for the Real-Time Monitoring of Modern Power Systems. *IEEE Access* **2022**, *10*, 29287–29306. . [CrossRef]
11. Ning, J.; Sarmadi, S.A.N.; Venkatasubramanian, V. Two-Level Ambient Oscillation Modal Estimation from Synchrophasor Measurements. *IEEE Trans. Power Syst.* **2015**, *30*, 2913–2922. [CrossRef]
12. Trudnowski, D.J.; Pierre, J.W. Overview of algorithms for estimating swing modes from measured responses. In Proceedings of the 2009 IEEE Power & Energy Society General Meeting, Calgary, AB, Canada, 26–30 July 2009; pp. 1–8. [CrossRef]
13. ACTIVATE. Ancillary Services in Active Distribution Networks, Based on Monitoring and Control Techniques. Available online: https://activate.ee.duth.gr/ (accessed on 7 March 2023).
14. Pippi, K.D.; Kryonidis, G.C.; Nousdilis, A.I.; Papadopoulos, T.A. A unified control strategy for voltage regulation and congestion management in active distribution networks. *Electr. Power Syst. Res.* **2022**, *212*, 108648. [CrossRef]
15. Pippi, K.D.; Kryonidis, G.C.; Nousdilis, A.I.; Papadopoulos, T.A. Assessing the Provision of Ancillary Services Considering BES Capacity Degradation. In Proceedings of the 2022 International Conference on Smart Energy Systems and Technologies (SEST), Eindhoven, The Netherlands, 5–7 September 2022; pp. 1–6. [CrossRef]
16. Li, X.; Hui, D.; Lai, X. Battery Energy Storage Station (BESS)-Based Smoothing Control of Photovoltaic (PV) and Wind Power Generation Fluctuations. *IEEE Trans. Sustain. Energy* **2013**, *4*, 464–473. [CrossRef]
17. de la Parra, I.; Marcos, J.; García, M.; Marroyo, L. Control strategies to use the minimum energy storage requirement for PV power ramp-rate control. *Solar Energy* **2015**, *111*, 332–343. [CrossRef]
18. Malamaki, K.-N.D.; Casado-Machado, F.; Barragán-Villarejo, M.; Gross, A.M.; Kryonidis, G.C.; Martinez-Ramos, J.L.; Demoulias, C.S. Ramp-Rate Limitation Control of Distributed Renewable Energy Sources via Supercapacitors. *IEEE Trans. Ind. Appl.* **2022**, *58*, 7581–7594. [CrossRef]

19. Blanco, C.; Reigosa, D.; Vasquez, J.C.; Guerrero, J.M.; Briz, F. Virtual Admittance Loop for Voltage Harmonic Compensation in Microgrids. *IEEE Trans. Ind. Appl.* **2016**, *52*, 3348–3356. [CrossRef]
20. Mokhtari, G.; Nourbakhsh, G.; Ghosh, A. Smart Coordination of Energy Storage Units (ESUs) for Voltage and Loading Management in Distribution Networks. *IEEE Trans. Power Syst.* **2013**, *28*, 4812–4820. [CrossRef]
21. Brenna, M.; De Berardinis, E.; Delli Carpini, L.; Foiadelli, F.; Paulon, P.; Petroni, P.; Sapienza, G.; Scrosati, G.; Zaninelli, D. Automatic Distributed Voltage Control Algorithm in Smart Grids Applications. *IEEE Trans. Smart Grid* **2013**, *4*, 877–885. [CrossRef]
22. EPRI. *Power Systems Dynamics Tutorial*; EPRI: Palo Alto, CA, USA, 2009, p. 1016042.
23. IEEE 39-Bus System. Available online: https://icseg.iti.illinois.edu/ieee-39-bus-system/ (accessed on 3 February 2023).
24. Baran, M.E.; Wu, F. Network reconfiguration in distribution systems for loss reduction and load balancing. *IEEE Trans. Power Del.* **1989**, *4*, 1401–1407. [CrossRef]
25. European Low Voltage Test Feeder. Available online: https://cmte.ieee.org/pes-testfeeders/resources/ (accessed on 1 April 2021).
26. Dugan, R.C.; Montenegro, D. *Reference Guide: The Open Distribution System Simulator*; EPRI: Palo Alto, CA, USA, 2020.
27. National Renewable Energy Laboratory. Commercial and Residential Hourly Load Profiles for all TMY3 Locations in the United States. 2014. Available online : https://data.openei.org/submissions/153 (accessed on 3 February 2023) .
28. Pfenninger, S.; Staffell, I. Long-term patterns of European PV output using 30 years of validated hourly reanalysis and satellite data. *Energy* **2016**, *114*, 1251–1265. [CrossRef]
29. DIgSILENT GmbH. DIgSILENT Solutions PowerFactory Version 20 .
30. Electrical Simulation Models–Generic Models. *IEC Wind Energy Generation Systems Part 27-1*. 2020.
31. Meersman, B.; Renders, B.; Degroote, L.; Vandoorn, T.; Vandevelde, L. Three-phase inverter-connected DG-units and voltage unbalance. *Electr. Power Syst. Res.* **2011**, *81*, 899–906. [CrossRef]
32. *IEEE Std 1547-2018 (Revision of IEEE Std 1547-2003)*; IEEE Standard for Interconnection and Interoperability of Distributed Energy Resources with Associated Electric Power Systems Interfaces. IEEE: New York, NY, USA, 2018; pp. 1–138.
33. Karlsson, D.; Hill, D. Modelling and identification of nonlinear dynamic loads in power systems. *IEEE Trans. Power Syst.* **1994**, *9*, 157–166. [CrossRef]
34. Milanovic, J.V.; Yamashita, K.; Martínez, S.V.; Djokic, S.Z.; Korunović, L.M. International Industry Practice on Power System Load Modeling. *IEEE Trans. Power Syst.* **2013**, *28*, 3038–3046. [CrossRef]
35. Pasiopoulou, I.; Kontis, E.; Papadopoulos, T.; Papagiannis, G. Effect of load modeling on power system stability studies. *Electr. Power Syst. Res.* **2022**, *207*, 107846. [CrossRef]
36. Kundur, P. *Power System Stability and Control*; McGraw-Hill: New York, NY, USA, 1994.
37. CIGRE. Benchmark systems for network integration of renewable and distributed energy resources. *CIGRE Task Force C6.04.02*. 2014.
38. Kontis, E.O.; Nousdilis, A.I.; Papagiannis, G.K.; Syed, M.H.; Guillo-Sansano, E.; Burt, G.M.; Papadopoulos, T.A. Power Hardware-in-the-Loop Setup for Developing, Analyzing and Testing Mode Identification Techniques and Dynamic Equivalent Models. In Proceedings of the 2019 IEEE Milan PowerTech, Milan, Italy, 23–27 June 2019.